Real-space self-consistent mean-field theory study of ABC star triblock copolymers

Weihua Li,[1,a)] Yuci Xu,[1] Guojie Zhang,[1] Feng Qiu,[1] Yuliang Yang,[1] and An-Chang Shi[2]
[1]*Department of Macromolecular Science, The Key Laboratory of Molecular Engineering of Polymers, Ministry of Education, China, Fudan University, Shanghai 200433, China*
[2]*Department of Physics and Astronomy, McMaster University, Hamilton, Ontario L8S 4M1, Canada*

(Received 1 June 2010; accepted 6 July 2010; published online 12 August 2010)

The phase behavior of ABC star triblock copolymers is examined using real-space self-consistent mean-field theory. The central part of the triangular phase diagram for ABC triblock copolymers with equal A/B, B/C, and C/A interactions is determined by comparing the free energy of a number of candidate ordered phases. In this region of the phase diagram, the dominant microstructures are cylinders with polygonal cross sections or two-dimensional polygon-tiling patterns. Most of the known polygon-tiling patterns observed in experiments and simulations, plus some neighboring morphologies, are considered in the construction of the phase diagram. The resulting phase behavior is consistent with experiments and computer simulations. © *2010 American Institute of Physics*. [doi:10.1063/1.3469857]

I. INTRODUCTION

Due to their ability to self-assemble into a variety of ordered microstructures, block copolymers provide a platform for the development of fabrication techniques of functional materials. Potential applications include lithographic templates for nanowires, photonic crystals, and high density magnetic storage media.[1] Recently, the manufacturing of large-scale ordered patterns by means of the self-assembly of block copolymers under the direction of patterned substrates[2–6] has attracted increasing interest in scientific community. This technology has the potential to decrease the cost of lithography of sub-30-nm patterns, which is required for improved data storage and computing speed in semiconductor technologies.

The development of nanomanufacturing technology using block copolymers requires a good understanding of the phase behavior of the block copolymers. The self-assembly of block copolymers is driven by the various interactions between the different blocks and the topological constraint of the block copolymer architecture. The equilibrium phases are a result of the delicate balance between these competing factors. Depending on the block copolymer architecture and block-block interactions, a variety of ordered microphases can be formed. Even for the simplest case of AB diblock copolymers, a number of ordered phases have been obtained, including lamellae, cylinders, spheres, and two networked (gyroid and *Fddd*) phases.[7–10] The number and complexity of ordered phases increases dramatically when block copolymers with more types of monomers and more complex architectures are used. For example, adding a chemically different C block onto an AB diblock copolymer chain leads to ABC triblock copolymers. Furthermore, the sequence and topology of ABC block copolymers can influence their ordered phases. Specifically, ABC triblock copolymers can assume a simple linear ABC topology by connecting the three blocks sequentially, or the three ends of the blocks can be linked at one junction point to form an ABC star triblock copolymer. Compared with AB diblock copolymers, the phase behavior of either ABC linear or ABC star triblock copolymers becomes much more complicated.[10,11] In AB diblock copolymers, the phase behavior is controlled by two main parameters: the A block composition f and the product χN of the polymerization N and the Flory–Huggins interaction parameter χ which characterizes the interaction between the two species. However, for the three-component ABC triblock copolymers, the parameters increase from two to five, including three interaction parameters $\chi_{AB}N$, $\chi_{AC}N$, and $\chi_{BC}N$, and two independent volume fractions f_A and f_B. Therefore, their phase diagrams become five dimensional. This feature makes ABC triblock copolymers be good model systems for the engineering of interesting structures which are not observed in AB diblock copolymers. On the other hand, the complexity of ABC block copolymers makes the exploration of the whole phase diagrams a formidable task. Besides the extra interaction parameters, the architecture and sequence of ABC triblock copolymers play a significant role in the self-assembling structures. For a given set of $\chi_{AB}N$, $\chi_{AC}N$, and $\chi_{BC}N$, linear ABC and ACB triblock copolymers have quite different phase behaviors.[10,12] Similarly, the self-assembly of an ABC star triblock copolymer melt is very different from that of a linear ABC triblock copolymer melt. In this paper, we will focus on the phase behavior of ABC star triblock copolymers.

The rich phase behavior of ABC star triblock copolymers has attracted considerable attention. A series of experiments have been carried out to study the formation of different morphologies[13–26] since the first three-miktoarm star copolymers were synthesized in 1992 by Iatrou and Hadjichristidis[27] and by Fujimoto *et al.*[28] A large number of

[a)]Author to whom correspondence should be addressed. Electronic mail: weihuali@fudan.edu.cn.

microphases have been observed in these experiments. In 2002, a systematical study was carried on the self-assembling of a set of ABC star triblock copolymers of the type $A_xB_{1.0}C_{1.0}$ with $0.2<x<25$ by Gemma *et al.*[11] using Monte Carlo (MC) simulations. These authors focused on polygonal-tiling patterns, which are cylindrical phases with polygonal cross sections. These two-dimensional tiling patterns are formed when the three blocks are immiscible and the blocks are long enough so that the three-arm junctions are localized on straight lines. Gemma *et al.* observed that, for x increasing from about 0.4 to 2.5, the two-dimensional (2D) tiling patterns follow the sequence [8.8.4], [6.6.6], [8.6.4; 8.6.6], [10.6.4; 10.6.6], and [12.6.4], where the 2D tiling patterns are designated by a set of integers indicating the sequence of polygons meeting at a vortex. These tiling patterns have been observed in experiments of Matsushita *et al.*[29] Furthermore, some of 2D tiling patterns predicted by the MC simulations have also been obtained in the dissipative particle dynamics simulations (DPD) by Huang *et al.*[30] Very recently, two-dimensional tiling patterns of ABC star triblock copolymers have been investigated using the self-consistent field theory by Zhang *et al.*[31] Despite these previous experimental and theoretical studies, a comprehensive understanding of ABC star triblock copolymers is still lacking.

From a theoretical point of view, the phase diagram of a given block copolymer system is constructed by comparing the free energy of different ordered phases. Due to a large number of studies, it has been well established that the self-consistent mean-field theory (SCMFT) provides a powerful theoretical framework for the study of the phase behavior of block copolymers.[7,32,33] In particular, SCMFT can be used to determine the relative stability of different phases because it provides accurate estimate of the free energy. The essence of the SCMFT is that the free energy of the system can be written as a functional of the spatially varying polymer concentrations and a set of conjugate fields. The equilibrium phases of the system corresponds to the polymer concentrations and conjugate fields which minimize the free energy, leading to a set of nonlinear equations or the SCMFT equations. In most cases, this set of SCMFT equations must be solved numerically to obtain solutions corresponding to different ordered phases. In the past years, two complementary methods to solve the SCMFT equations have been developed. In the first class of methods, or the spectral methods, the spatially varying functions are expanded in terms of a set of basis functions, leading to a set of algebraic equations for the expansion coefficients. In the second class of methods, or the real-space methods, the space is discretized and the differential equations are solved using different numerical schemes. The spectral method has been very successful in computing the free energy of an ordered phase if the symmetry of the ordered phase is known, as first demonstrated by Matsen and Schick.[7] It should be emphasized that although the initial application of the spectral method utilizes the symmetry of the ordered phases, the spectral method is a generic numerical method which is capable of predicting new ordered phases once the symmetry restriction on the basis functions is relaxed, as demonstrated for the case of linear ABC triblock copolymers by Guo *et al.*[12] Recently, Zhang *et al.*[31] have applied the spectral method to ABC star triblock copolymers, revealing a rich array of two-dimensional tiling patterns. Parallel to the spectral methods, real-space methods to solve the SCMFT equations of polymers have been developed, notably by Drolet and Fredrickson.[34] In recent years, the real-space methods have benefited tremendously from the development of a highly efficient algorithm solving the modified diffusion equations, the operator-split algorithm as a second-order method (OpS2) developed by Tzeremes *et al.*[35,36] Furthermore, this algorithm can be readily parallelized by using the FFTW package for the fast-Fourier transformations. In addition, the operator-split algorithm has been developed into a fourth-order backward-differentiation-formula scheme with more confidential accuracy for the free energy.[37] A generic strategy of studying phases and phase transitions of complex block copolymer systems can be developed by combining the spectral and real-space methods. First of all, the generic spectral methods and large-scale real-space methods can be used to produce a set of candidate structures. These candidate phases can then be used as initial conditions in the more accurate spectral or real-space methods to obtain accurate free energies.

In this work, we apply the strategy of combining the real-space and the generic spectral methods to ABC star triblock copolymer melts. Specifically, the generic spectral method of Guo *et al.*[12] is first used as a screening technique to obtain a set of candidate phases. These candidate structures are then used as the initial conditions for the real-space method. In order to broaden the scope of the search, initial conditions include some additional morphologies obtained from experiments and computer simulations. The resulting free energy of the different ordered phases are used to construct phase diagrams of the system.

II. THEORY

We consider an incompressible melt of ABC star triblock copolymers with a degree of polymerization N in a volume of V and the chain lengths of A, B, and C blocks are f_AN, f_BN, and $f_CN(f_A+f_B+f_C=1)$, respectively. Spatial lengths in our calculations are expressed in units of the radius of gyration R_g of the polymer. Within the mean-field approximation to statistical mechanics of the Edwards model of polymers,[32,33] at a temperature T, the free energy functional F for n Gaussian triblock copolymer chains is

$$\frac{F}{nk_BT} = -\ln Q + \frac{1}{V}\int d\mathbf{r}\{\chi_{AB}N\phi_A(\mathbf{r})\phi_B(\mathbf{r}) + \chi_{AC}N\phi_A(\mathbf{r})\phi_C(\mathbf{r}) + \chi_{BC}N\phi_B(\mathbf{r})\phi_C(\mathbf{r}) - \omega_A(\mathbf{r})\phi_A(\mathbf{r}) - \omega_B(\mathbf{r})\phi_B(\mathbf{r}) - \omega_C(\mathbf{r})\phi_C(\mathbf{r}) - \eta(\mathbf{r})[1-\phi_A(\mathbf{r})-\phi_B(\mathbf{r})-\phi_C(\mathbf{r})]\}, \quad (1)$$

where ϕ_A, ϕ_B, and ϕ_C are the monomer densities. The partition function Q is for a single polymer chain interacting with the mean fields of ω_A, ω_B, and ω_C produced by the surrounding chains. The interactions among the three dissimilar monomers are characterized by three Flory–Huggins

interaction parameters, χ_{AB}, χ_{AC}, and χ_{BC}. Minimization of the free energy with respect to the monomer densities and the mean fields leads to the following standard mean-field equations[33]

$$\begin{aligned}
&\omega_A(\mathbf{r}) = \chi_{AB}N\phi_B(\mathbf{r}) + \chi_{AC}N\phi_C(\mathbf{r}) + \eta(\mathbf{r}),\\
&\omega_B(\mathbf{r}) = \chi_{AB}N\phi_A(\mathbf{r}) + \chi_{BC}N\phi_C(\mathbf{r}) + \eta(\mathbf{r}),\\
&\omega_C(\mathbf{r}) = \chi_{AC}N\phi_A(\mathbf{r}) + \chi_{BC}N\phi_B(\mathbf{r}) + \eta(\mathbf{r}),\\
&\phi_A(\mathbf{r}) = \frac{1}{Q}\int_0^{f_A} ds q_A(\mathbf{r},s)q_A^\dagger(\mathbf{r},s),\\
&\phi_B(\mathbf{r}) = \frac{1}{Q}\int_0^{f_B} ds q_B(\mathbf{r},s)q_B^\dagger(\mathbf{r},s),\\
&\phi_C(\mathbf{r}) = \frac{1}{Q}\int_0^{f_C} ds q_C(\mathbf{r},s)q_C^\dagger(\mathbf{r},s),\\
&Q = \frac{1}{V}\int d\mathbf{r} q_K(\mathbf{r},s)q_K^\dagger(\mathbf{r},s),\\
&\phi_A(\mathbf{r}) + \phi_B(\mathbf{r}) + \phi_C(\mathbf{r}) = 1.
\end{aligned} \tag{2}$$

In the above equations, $q_K(\mathbf{r},s)$ and $q_K^\dagger(\mathbf{r},s)(K=A,B,C)$ are end-segment distribution functions which have standard definitions.[33] These distribution functions satisfy the modified diffusion equations

$$\frac{\partial q_K(\mathbf{r},s)}{\partial s} = \nabla^2 q_K(\mathbf{r},s) - \omega_K(\mathbf{r},s)q_K(\mathbf{r},s), \tag{3}$$

$$-\frac{\partial q_K^\dagger(\mathbf{r},s)}{\partial s} = \nabla^2 q_K^\dagger(\mathbf{r},s) - \omega_K(\mathbf{r},s)q_K^\dagger(\mathbf{r},s). \tag{4}$$

The initial conditions are $q_K(\mathbf{r},0)=q_L^\dagger(\mathbf{r},0)q_M^\dagger(\mathbf{r},0)$, where $(KLM)\in\{(ABC),(BCA),(CAB)\}$ and $q_K^\dagger(\mathbf{r},f_K)=1$. For numerical solutions, we employ the second-order operator-split method[35,36] to solve the modified diffusion equations for the end-segment distribution functions. In our real-space calculations, the ABC star copolymer chains are placed in a rectangle box with sizes of $L_x\times L_y$ for 2D systems and a rectangular cuboid box of $L_x\times L_y\times L_z$ for three-dimensional (3D) systems. Periodic boundary conditions are imposed automatically on each direction of the box. The grid spacing is chosen as small enough to ensure that it influences the free energy with errors smaller than 10^{-8}. The total chain contour is discretized into 10^3 points.

III. RESULTS AND DISCUSSION

To focus on the influence of the compositions on the phase behaviors, we fix the interactions between different blocks as $\chi_{AB}N=\chi_{AC}N=\chi_{BC}N=60$. In previous works, the weak and strong segregation cases have been examined with SCMFT by Zhang *et al.* and with MC by Gemma *et al.*,[11] respectively. Their work suggests that the formation of polygon-tiling patterns are common. Therefore, we choose the intermediate segregation case which bridges the former two cases. It is known that the real-space method to solve the diffusion equations requires a high degree of discretization to obtain high accuracy of free energy,[37] especially in the strong segregation phase region. In other words, the free energy is sensitive to the discretization of the chain contour, $\Delta s = 1/N_s$, where 1 is the rescaled contour length by N and N_s is the total discretized points along the chain. Cochran and co-workers[37] have carefully studied the influence of Δs for diblock copolymers in the strong segregation region. With the OpS2 approach, a small Δs $(<10^{-3})$ is required to obtain a reliable accuracy of free energy. However, the phase transition is not determined directly by the absolute value of free energy, but by its relative value of different phases. Because the phase transitions are determined by the free energy differences between the different phases, the determination of the phase diagram may be insensitive to the absolute accuracy of the free energy, particularly for the situation of weak or intermediate segregation. In order to give a quantitative description of this observation, we calculate the phase transitions between the bcc and hex phases of diblock copolymers, which have been accurately determined with the spectral method by Matsen,[38] by using the OpS2 approach. Three interaction parameters of the AB diblock copolymer, $\chi N=20$, 40, and 60, are considered in our calculations. Each phase transition point is identified with two different discretizations of $\Delta s=10^{-2}$ and $\Delta s=10^{-3}$. The results are present in Table I. The results of the phase transitions obtained by OpS2 are present as five-digit decimals and those of the spectral method from Fig. 2 of Ref. 38 are shown as three-digit decimals. We can find that the influence of Δs varying from 10^{-2} to 10^{-3} on the phase transition boundary is very small $(\Delta f \lesssim 10^{-4})$ for various $\chi N=20$, 40, and 60, although the accuracy of the free energy depends more strongly on Δs. This phenomenon is also seen in our previous work.[39] The small error in the phase boundary is not significant either in theoretical calculations or in experiments. For the present system of ABC triblock copolymers, we will show that the dependence of the phase transitions on Δs is also neglectably small in the following paragraphs. Therefore, we decided that $\Delta s=10^{-3}$ as a reasonable discretization in the calculations of the phase diagram of the triblock copolymers.

TABLE I. The phase transition boundaries between the bcc and hex phases obtained by the OpS2 with discretizations $\Delta s=10^{-2}$ and $\Delta s=10^{-3}$, together with the free energy difference of the bcc phase between the two discretizations in AB diblock copolymers. The transition data read from Fig. 2 in Ref. 38 is shown as a reference.

χN	$f_{bcc-hex}$ $\Delta s=10^{-2}$	$f_{bcc-hex}$ $\Delta s=10^{-3}$	$f_{bcc-hex}$ of Ref. 38	$\Delta F_{bcc}/nk_BT$
20	0.243 40	0.243 37	0.243	2×10^{-4}
40	0.166 13	0.166 11	0.166	3×10^{-4}
60	0.141 77	0.141 67	0.141	2×10^{-3}

There are two main steps in the construction of the phase diagrams. The first step is to select possible candidate structures. The predicted structures by the generic spectral methods in Ref. 31 are used as candidate phases. In addition, some morphologies observed in experiments and computer

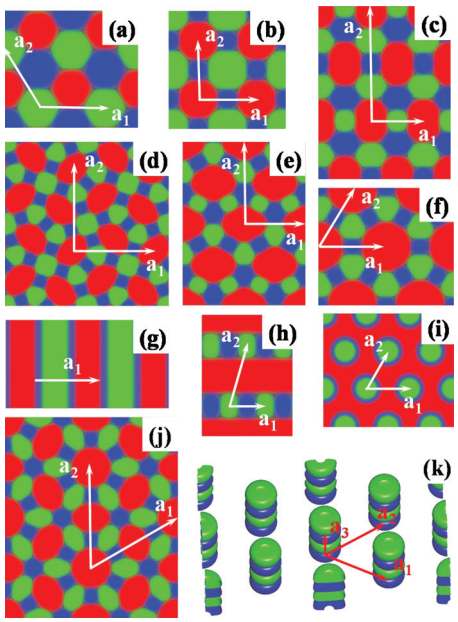

FIG. 1. Monomer density plots of typical ordered microstructures formed in ABC star triblock copolymers with $\chi_{AB}N=\chi_{AC}N=\chi_{BC}N=60$. The colors of red, green, and blue, indicate the regions where the most components are A, B, and C, respectively. There are seven 2D cylindrical structures of polygon-tiling patterns with translational symmetry along the third direction: (a) [6.6.6], (b) [8.8.4], (c) [8.6.4; 8.6.6], (d) [10.6.4; 10.8.4], (e) [10.6.4; 10.6.6], (f) [12.6.4], and (j) [8.6.4; 8.6.6; 12.6.4] (these integers indicate the sequence of polygons meeting at a vortex in each pattern); and three other 2D structures, including (g) L3, (h) HL and hexagonally arranged HC, and one HHC. The basic vectors of these periodic structures are labeled as a_i (i =1,2,3).

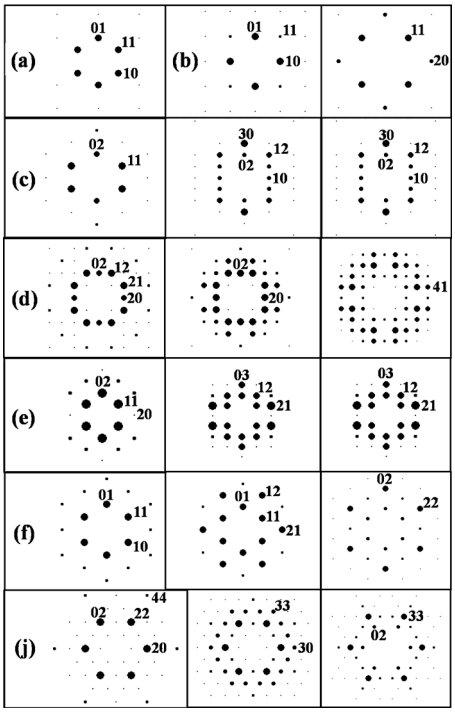

FIG. 2. Typical Fourier spectra of the density profiles of (a)–(f) and (j) in Fig. 1. The size of the filled circles denotes the peak intensities. For (a), the picture is for A (red), B (green), or C (blue) component; for (b), the left picture is for A or B, and the right one is for C; for others, the pictures from left to right are for A, B, and C, respectively. For each pattern, some typical diffraction peaks are labeled.

simulations are produced by using some special initial conditions. The second step is to identify the stabilities of these structures by comparing their free energies obtained by the real-space method. For each given set of block compositions, or a given point in the triangular phase diagram, all possible candidate structures from the previous theoretical and experimental studies are considered. In our real-space calculations, usually a rectangular box composed of one or two unit cells are simulated; a lattice of 128×128 is used to discretize the 2D box and, accordingly, the grid spacing along either x or y directions is smaller than $0.1R_g$. For 3D structures, the lattice is chosen as 64^3 and the grid spacing is still kept as smaller than $0.1R_g$.

The candidate structures in our calculations are present in Fig. 1. Among these candidate phases, the cylindrical structures, or polygon-tiling patterns, with translational symmetry along the third direction, including [6.6.6], [8.8.4], [8.6.4; 8.6.6], [10.6.4; 10.8.4], [10.6.4; 10.6.6], [8.6.4; 8.6.6; 12.6.4], and [12.6.4], are the 2D phases. Besides these polygonal structures, additional three 2D structures, i.e., three-color lamellae (L3), the core-shell cylinders (HC), and hierarchical lamellae (HL), are considered to determine the phase diagrams together with one 3D structure of hierarchical cylinders (HHC) [Fig. 1(k)]. Note that these structures can have their mirror phases when the compositions are cycling. For example, the main component contained in the square domains of [8.8.4] can be A (red), or B (green), or C (blue). In our previous work,[39] we have discussed that there are other possible morphologies for the hierarchical lamellae such as zero-shift hierarchical lamellae whose free energy is very close to that of the 180°-shift HL in Fig. 1(h) when $\chi_{AB}N=\chi_{AC}N=\chi_{BC}N=60$. The free energy difference as small as 10^{-7} can hardly influence the phase boundaries between HL and other phases. Therefore, here we only consider the 180°-shift morphology of HL. Similarly, the shift of B/C domains among neighbor cylinders in the structures of the hierarchical cylinders is possible.[11] For the hexagonally arranged cylinders, the packing of B/C domains with 180-degree shifts among neighbor cylinders is frustrated. In addition, according to the similar reason in HL, the free energy difference induced by the appearance of the shift in HHC should be very small, too. To avoid the frustration, it is reasonable to include only the zero-shift morphology of HHC into the construction of the phase diagram. The basic vectors of these periodic structures are denoted as a_i (i=1, 2, and 3). These structures, including [12.6.4], [8.6.4; 8.6.6; 12.6.4], HC, and HHC, have sixfold symmetry with $a_1=a_2$; the structures of [8.8.4] and [10.6.4; 10.8.4] have fourfold symmetry with $a_1=a_2$; and the structure of [6.6.6] has threefold symmetry with $a_1=a_2$. However, the structures of [8.6.4; 8.6.6] and [10.6.4; 10.6.6] have rectangular unit cells with $a_1\neq a_2$ and the structure of HL has a parallelogrammic unit cell with $a_1\neq a_2$.

To show the symmetries of the 2D structures shown in Fig. 1, their Fourier spectra $\phi_k(\mathbf{q})$ (k=A,B,C) are calculated and are given in Fig. 2. The radii of filled circles denote the peak intensities. From left to right of (c), (d), (e), (f), and (j), the patterns are for $\phi_A(\mathbf{q})$, $\phi_B(\mathbf{q})$, and $\phi_C(\mathbf{q})$, respectively. The three densities of [6.6.6] have the similar spectrum pat-

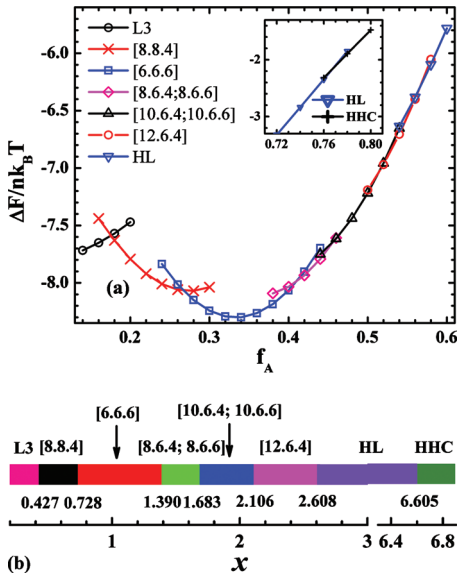

FIG. 3. (a) Free energy differences from the value of the homogeneous phase as a function of the volume fraction of A composition for ABC star triblock copolymers with symmetric B and C arms. With f_A increasing, the phase structure sequence is from L3, through [8.8.4], [6.6.6], [8.6.4; 8.6.6], [10.6.4; 10.6.6], [12.6.4], HL, to HHC. The inset shows the transition between HL and HHC. (b) Phase stability regions as a function of the arm-length ratio of $x=f_A/f_B$. Note that one break is applied with the x axis for the reason of clarity of the figure.

tern of Fig. 2(a), the A and B densities of [8.8.4] have the similar spectrum pattern of the left one in Fig. 2(b), and the spectrum of the C density is the right one. Although the peak intensities of small-angle x-ray scattering (SAXS) patterns are the summation of the contributions from three components in experiments, these calculated spectrums can be used to explain experimental SAXS patterns qualitatively, particularly useful for these complex 2D polygonal structures. The peak intensities of {21} of $\phi_A(\mathbf{q})$ and $\phi_B(\mathbf{q})$ in Fig. 2(d) are the largest and that of {20} of $\phi_A(\mathbf{q})$ is weaker. This observation is consistent with the relative intensity of {21} and {20} peaks in Fig. 4 of Ref. 23. Other SAXS patterns of Figs. 2, 3, and 5 in Ref. 23 and Figs. 4 and 8 in Ref. 24 can also be well explained by these Fourier spectrums.

In the MC simulations by Gemma *et al.*[11] and experiments,[20,23] two of the three arms are kept to be equal length and the arm-length ratio is expressed as $1:1:x$. We start with the calculation of the phase stability along this phase path. Here we assume that B and C arms have equal length and the A arm holds the arm-length ratio of $x=f_A/f_B$. The free energy differences of candidate phases from the value of the homogeneous phase as a function of the volume fraction f_A are given in Fig. 3(a) as well as the phase stability region as a function of x in Fig. 3(b). In the free energy plot, the free energy of some metastable phases are not shown, such as that of HC in the region of $0.74 \leq f_A \leq 0.8$, where HC has higher free energy than HL or HHC. Consistent with the MC results, two 3D structures, i.e., the lamellae+spheres and lamellae in spheres, are not included in our calculations. These two phases are located at the two ends of the region of small x (around 0.2) and large x (around 20), respectively. For our choice of interactions, the two regions are very small and it would not influence the central part of the phase diagram much which is the most interesting region for ABC star copolymers. With increasing x, the phase sequence composed of L3, [8.8.4], [6.6.6], [8.6.4; 8.6.6], [10.6.4; 10.6.6], [12.6.4], HL, and HHC is consistent with that of MC simulation. Furthermore, the phase boundaries are also in agreement with those of MC qualitatively. As MC cannot determine the free energy directly, the phase region can just be estimated from the equilibrium energy. However, the SCMFT can identify the phase stability region by calculating the free energy. The phase regions of [8.8.4], [6.6.6], [8.6.4; 8.6.6], [10.6.4; 10.6.6], [12.6.4], and HL are $0.427 \leq x \leq 0.728$, $0.728 \leq x \leq 1.390$, $1.390 \leq x \leq 1.683$, $1.683, \leq x \leq 2.106$, $2.106 \leq x \leq 2.608$, and $2.608 \leq x \leq 6.605$, respectively. Along this phase path, experimentalists synthesized a set of copolymers, and observed their self-assembling microstructures by using SAXS and transition electron microscopy (TEM) measurements. In experiments by Takano *et al.*,[20] three ABC star terpolymers, composed of polystyrene (S), polyisoprene (I), and poly(2-vinylpyridine) (P), are investigated with volume ratios of 1:1:0.7, 1:1:1.2, and 1:1:1.9, respectively. The formed structures of $I_{1.0}S_{1.0}P_{0.7}$, $I_{1.0}S_{1.0}P_{1.2}$, and $I_{1.0}S_{1.0}P_{1.9}$, are [6.6.6], [8.8.4], and [12.6.4], respectively. Although, the corresponding sequence of the structures in our SCMFT calculations is [8.8.4], [6.6.6], and HL, the locations of these structures are not far away from our phase regions, especially for [6.6.6] and [12.6.4]. The discrepancy between theoretical results and experimental observations can be attributed to the different interactions, different monomer sizes, and polydispersity.

To testify the influence of Δs on the phase transitions of the morphologies formed in the ABC star copolymers, here we calculate the phase transition between [10.6.4; 10.6.6] and [12.6.4] along the symmetric axis of $f_B=f_C$ with two different values of $\Delta s=0.001$ and $\Delta s=0.005$. The results of the free energy together with the free energy difference, defined as $F_{diff}=F_{[10.6.4;10.6.6]}-F_{[12.6.4]}$, are present in Table II. The transition points, estimated by linearly interpolating the free energy difference as a function of f_A from the data of

TABLE II. The free energies of [10.6.4; 10.6.6] and [12.6.4], as well as their free energy difference calculated with $\Delta s=0.001$ and $\Delta s=0.005$, respectively.

	[10.6.4; 10.6.6] $\Delta s=0.005$	[12.6.4] $\Delta s=0.005$	$\Delta s=0.005$	[10.6.4; 10.6.6] $\Delta s=0.001$	[12.6.4] $\Delta s=0.001$	$\Delta s=0.001$
f_A	F/nk_BT	F/nk_BT	F_{diff}/nk_BT	F/nk_BT	F/nk_BT	F_{diff}/nk_BT
0.51	11.496 881	11.504 342	0.007 461	11.502 275	11.509 710	0.007 435
0.52	11.469 376	11.457 015	−0.012 361	11.474 692	11.462 265	−0.012 4273

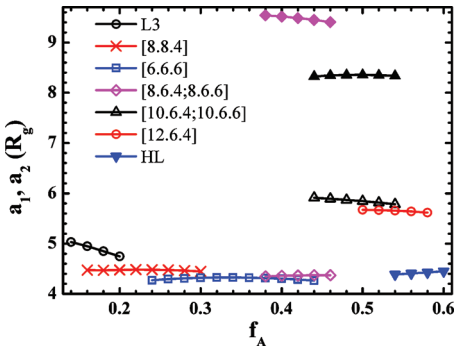

FIG. 4. The magnitudes of basic vectors in unit of the radius of gyration R_g of these 2D structures along the phase path in Fig. 2. The unfilled (including the symbols of cross) and filled symbols denote the vector lengths of a_1 and a_2, respectively. For the reason of clarity, the a_1 of HL is not shown.

$\Delta s=0.001$ and $\Delta s=0.005$, are at $f_A=0.513\,74$ and $f_A=0.513\,76$, respectively. The influence of Δs on the transition point can be safely neglected.

The basic vectors play an important role during the measurements of the microstructures and can be determined by SAXS or TEM techniques in experiments. In solving the SCMFT equations, the free energy is minimized with respect to the box sizes which are related to the lengths of basic vectors by simple algebraic relations. Here, the magnitudes of the basic vectors of 2D structures are present in Fig. 4. a_1 is denoted by the unfilled symbols (including the cross symbols) and a_2 is denoted by the filled symbols when $a_1 \neq a_2$. Note that the value of a_1 for HL, which decreases from $2.796R_g$ to $1.621R_g$ when f_A increases from 0.54 to 0.78, is not shown in order to narrow the range of the magnitude for the reason of clarity of the figure. The magnitude of $a_1=a_2$ of [6.6.6] is slightly smaller than that of [8.8.4], and they do not have large change for varying volume fractions. For example, $a_1=a_2$ of [6.6.6] varies between about $4.265R_g$ and $4.327R_g$ with a maximum at $f_A=1/3$ when increasing $f_A=0.24$ to $f_A=0.44$. In experiments,[23] the lengths of basic vectors are measured as $a_1=80$ nm and $a_2=67$ nm for [6.6.6] of the copolymer $I_{1.0}S_{1.0}P_{0.7}$, and $a_1=59$ nm and $a_2=56$ nm for [8.8.4] of the copolymer $I_{1.0}S_{1.0}P_{1.2}$. Including the factor that $I_{1.0}S_{1.0}P_{0.7}$ has smaller molecular weight than $I_{1.0}S_{1.0}P_{1.2}$, a_1 or a_2 of [6.6.6] are notably larger than those of [8.8.4] in experiments. This feature is different from the prediction of our theoretical calculations. However, that $a_1=a_2$ of [12.6.4] is much larger than that of [8.8.4] or [6.6.6] in experimental measurements is qualitatively consistent with our theoretical results. For [8.6.4; 8.6.6] and [10.6.4; 10.6.6], a_2 is larger than a_1. The length ratios a_2/a_1 in the shown regions are larger than $\sqrt{3}$ for [8.6.4; 8.6.6] and are smaller than $\sqrt{3}$ for [10.6.4; 10.6.6]. This suggests that the octagons are elongated in [8.6.4; 8.6.6] and the decagons are compressed in [10.6.4; 10.6.6], along the direction of a_2. The deviations from the regular polygons for both [8.6.4; 8.6.6] and [10.6.4; 10.6.6] are reduced slightly as increasing f_A.

It can be helpful to split the free energy into two parts: internal (U) and entropic ($-TS$). The internal and entropic contributions to the free energy can be expressed as[8]

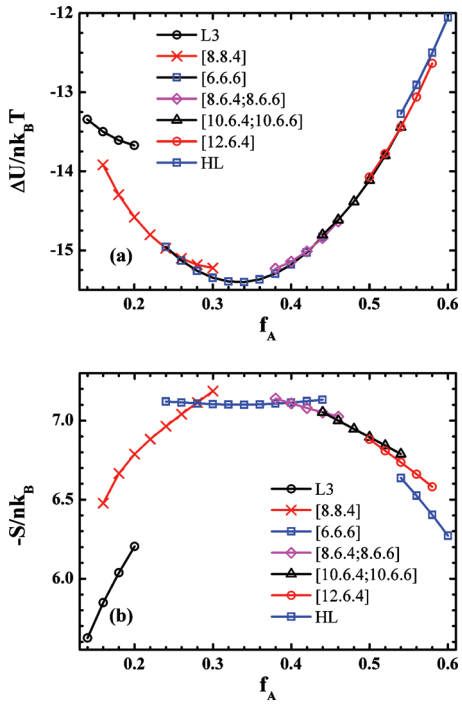

FIG. 5. (a) Internal part $\Delta U/nk_BT$ and (b) entropic part $-S/nk_B$ of the free energy difference $\Delta F/nk_BT$ in Fig. 2(a) as a function of f_A.

$$\frac{U}{nk_BT}=\frac{1}{V}\int d\mathbf{r}[\chi_{AB}N\phi_A(\mathbf{r})\phi_B(\mathbf{r})+\chi_{AC}N\phi_A(\mathbf{r})\phi_C(\mathbf{r})+\chi_{BC}N\phi_B(\mathbf{r})\phi_C(\mathbf{r})],$$
$$-\frac{S}{nk_B}=-\ln Q-\frac{1}{V}\int d\mathbf{r}[\omega_A(\mathbf{r})\phi_A(\mathbf{r})+\omega_B(\mathbf{r})\phi_B(\mathbf{r})+\omega_C(\mathbf{r})\phi_C(\mathbf{r})]. \quad (5)$$

$\Delta U/nk_BT$, the internal energy subtracted by that of the homogeneous phase, is shown in Fig. 5 together with the entropic energy of $-S/nk_B$. From Fig. 5(a), we can find that L3 has very high internal energy at small f_A which is induced by the penetrations of B and C arms through A domains. At the same time, L3 is favorable from the aspect of entropic energy, or the chain stretching energy, because the B and C arms can get the largest entropy in the lamellar structure when they have equal large lengths compared with the A arm. The combination of the two contributions make L3 be the stable phase when $f_A \lesssim 0.176$. When increasing f_A, the internal energy becomes more dominant on the entropic energy and the stable phase transfers from L3 to the phases of polygon-tiling patterns where the arm penetrations in dissimilar phase regions are diminished. After entering the 2D polygonal phases, the variation of the internal energy becomes smoother without obvious discontinuity. However, when the stable phase transfers from [12.6.4] to HL, a significant drop appears again. The reason is similar to that of the appearance of L3 as a stable phase.

On the above phase path, two of 2D polygonal phases, [10.6.4; 10.8.4] and [8.6.4; 8.6.6; 12.6.4], do not appear. To obtain the stability region of the two phases which have been observed in experiments, we turn to study another phase path

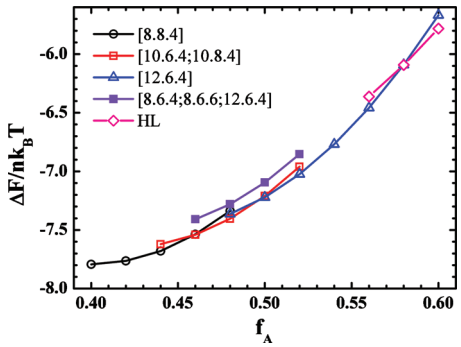

FIG. 6. The free energy difference $\Delta F/nk_BT$ as a function of f_A for fixed $f_C=0.2$. The phase of [8.6.4; 8.6.6; 12.6.4], denoted as filled squares, does not appear as stable one in this parameter region.

by varying f_A for fixed $f_C=0.2$. The free energy difference as a function of f_A varying from 0.4 to 0.6 is plotted in Fig. 6 and the corresponding lengths of the basic vectors are plotted in Fig. 7. Between the phases of [8.8.4] at $f_A=0.4$ and HL at $f_A=0.6$, [10.6.4; 10.8.4] and [12.6.4] appear as stable phases. The phase of [8.6.4; 8.6.6; 12.6.4] is metastable as its free energy is higher than that of [8.8.4], or [10.6.4; 10.8.4], or [12.6.4] between $f_A=0.46$ and $f_A=0.52$. From the tendency of the curve, it can be concluded that [8.6.4; 8.6.6; 12.6.4] would not become stable for wider phase region. This is justified by our following more systematical calculations of the phase diagram. From the plot of the lengths of the basic vectors, we can find that the length of basic vectors of [8.6.4; 8.6.6; 12.6.4] is as large as about $a_1=a_2=10R_g$, which is slightly larger than that of [10.6.4; 10.8.4], and it has a slow decreasing tendency as f_A increases. The large magnitude of the basic vector is resulted by the inserting of an octagonal A domain between two neighbor decagonal A domains. After splitting the free energy into internal energy and entropic energy with the formulas of Eq. (5) (see Fig. 8), the stability of [8.6.4; 8.6.6; 12.6.4] can be understood more readily. Although its internal energy is not much higher than that of [10.6.4; 10.8.4] or [12.6.4], but its entropic energy is significantly higher than that of other structures. The Archimedean polygon-tiling principle ensures [8.6.4; 8.6.6; 12.6.4] with reasonable low interfacial energy, which mainly composes the internal energy. From the density plot of Fig. 1(j), it can be seen that both the octagonal A domains and the hexagonal B domains are deformed from the shapes of their regular

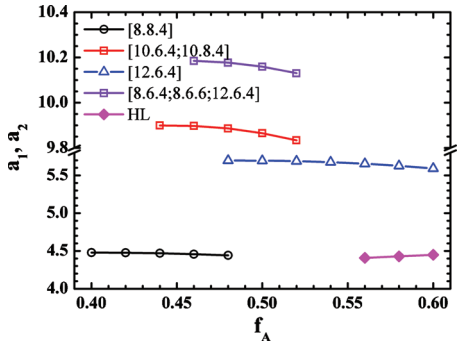

FIG. 7. The lengths of basic vectors as a function of f_A along the phase path of fixed $f_C=0.2$.

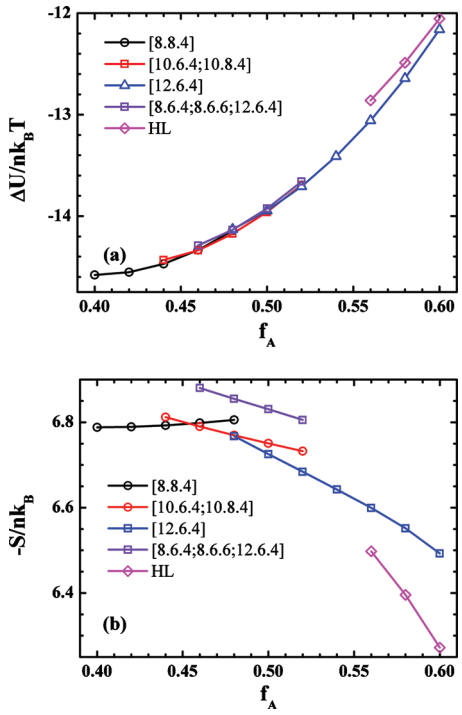

FIG. 8. (a) Internal energy of $\Delta U/nk_BT$ and (b) entropic energy of $-S/nk_B$ of various structures as a function f_A on the phase path of fixed $f_C=0.2$.

polygons. As a consequence, these deformations can induce nonuniform chain stretching which results in an entropic energy penalty.[8]

With the knowledge of these structures, the phase diagram can be determined by comparing the free energy among possible candidate structures. For the case of three equal interaction parameters, the triangular phase diagram is threefold symmetric and is mirror symmetric with its three axes of $f_A=f_B$, $f_A=f_C$, and $f_B=f_C$. Therefore, the calculation of the whole triangular phase diagram is reduced to one-sixth. The triangular phase diagram obtained by our SCMFT calculations is given in Fig. 9. To focus on the stability of 2D polygonal phases, only the central region of the phase diagram is determined. Six phase regions of the 2D polygonal phases are determined by calculating the transition boundaries between them and their surrounding phases. Besides the

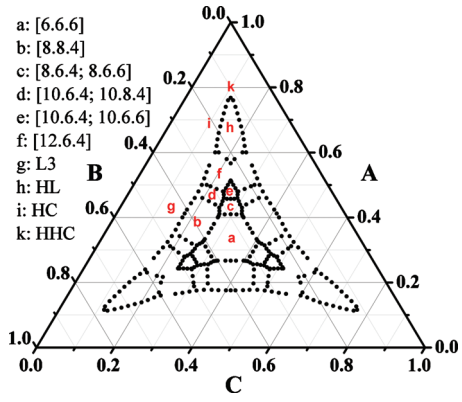

FIG. 9. The triangular phase diagram of ABC star triblock copolymers with equal interaction parameters of $\chi_{AB}N=\chi_{AC}N=\chi_{BC}N=60$. The phase diagram is composed of a set of transition points shown as black dots.

2D tiling patterns, three main surrounding structures, i.e., L3, HL, HC, are used to calculate their phase boundaries. In addition, the phase transition point between HL and the 3D hierarchical cylinders of HHC is given in Fig. 9. The phase regions of [12.6.4] and HL are calculated by comparing their free energy with that of L3 or HC without considering the possible existence of core-shell gyroid phase. According to the phase diagram of diblock copolymers,[37] the phase region of core-shell gyroid phase must be small for this degree of segregation if it exists. The phase of [8.6.4; 8.6.6; 12.6.4] do not appear as a stable phase in the considered phase regions. The stability of [8.6.4; 8.6.6; 12.6.4] has been analyzed in the above paragraph. The central part of the triangular phase diagram has a consistent shape with the whole phase diagram.

Two more phase paths, with fixed $f_B:f_C=1.8$ or $f_A:f_C=2$, are examined by experiments besides the symmetric phase path.[24] Some observed structures in experiments are not exactly located in the predicted phase regions of our phase diagram. Besides the factors mentioned previously, which may induce the discrepancies, there is another important factor in the experiments which is that many star copolymers are obtained by blending two kinds of copolymers, even adding additional I homopolymer. For example, $I_{1.0}S_{1.8}P_{2.9}$ are obtained by blending $I_{1.0}S_{1.8}P_{2.5}$ and $I_{1.0}S_{1.8}P_{3.2}$. The two lengths of the P arm can definitely influence the phase stabilities. Another important difference between our results and experiments is that [8.6.4; 8.6.6; 12.6.4], as a metastable phase in our calculations, is observed with $I_{1.0}S_{1.8}P_{2.0}$ in experiments. There are two main possible reasons for the experimental observation of [8.6.4; 8.6.6; 12.6.4]. The first one is that there is a considerable possibility to observe a metastable phase in experiments. The second one is that there are many differences between theoretical systems and experimental conditions mentioned before.

Although there is a discrepancy between our theoretical calculations and experimental observations, our results are in general agreement with most of other theoretical results of either SCMFT calculations or DPD simulations. Besides the early MC research on the symmetric phase path of $f_B=f_C$ by Gemma *et al.*,[11] for which careful comparisons have been given in the previous paragraph, a few more literatures have been devoted to the investigation of the phase diagram of ABC star copolymers in recent years. Tang *et al.*[40] estimated a phase diagram with $\chi_{AB}N=\chi_{AC}N=\chi_{BC}N=35$ by using 2D SCMFT calculations. In their phase diagram, the phases of [6.6.6], [8.8.4], HL, and L3, are located in the similar regions as ours although a few polygonal phases are missing. In 2008, Huang and co-workers carried DPD simulations on the structure formations of the copolymers and constructed a phase diagram in the Fig. 4 of Ref. 30. They observed more polygonal structures than Tang *et al.*[40] in similar phase regions as those in our phase diagram. In their simulations, two stable polygonal phases, [12.6.4] and [8.6.4; 8.6.6], are not observed. Very recently, Zhang *et al.* examined the phase behaviors of the triblock copolymers with the generic spectral method focusing on the discovery of new phases. Their phase diagram is qualitatively consistent with ours. However, there are obvious discrepancies. First, our phase diagram is much more detailed which can be seen from the shapes of phase boundaries. This difference is resulted by the limited accuracy of the free energy of the generic spectral method, which is more dependent on the number of basis functions than the traditional spectral method. Second, the polygonal phase of [10.6.4; 10.8.4] is not observed in their phase diagram.

IV. CONCLUSIONS

In conclusion, we have studied the phase behavior of ABC star triblock copolymers with $\chi_{AB}N=\chi_{AC}N=\chi_{BC}N=60$ by using the OpS2 real-space SCMFT calculations together with the generic spectral method. The spectral method is mainly used to search new structures and the real-space method is used to determine the stability regions of these observed structures. We test the reliability of the OpS2 approach with the phase transition between the bcc sphere phase and the hex cylinder phase of AB diblock copolymer. The comparisons of our real-space results of various discretization on the contour length with those of the spectral method indicate that the phase transition boundaries determined by the OpS2 approach are reliable even for the segregation as strong as $\chi N=60$. For the ABC star triblock copolymers, we mainly focus on the phase regions of 2D polygon-tiling patterns and include ten 2D phases and one 3D phase. We first determined the phase stability along the phase path with two equal arm lengths. Our results are well consistent with those of MC simulations. Then we calculated the phase regions along the phase path with fixed $f_C=0.2$. On this phase path, we analyzed the stability of [8.6.4; 8.6.6; 12.6.4] and found that it is a metastable phase. Finally, we constructed the triangular phase diagram with these candidate phases. Except for [8.6.4; 8.6.6; 12.6.4], there are ten stable phases composing the triangular phase diagram. In general, the phase regions predicted by our SCMFT calculations are in good agreement with other theoretical results of either SCMFT calculations or DPD simulations. However, our results are more detailed and comprehensive, and especially more phases are included in the phase diagram. By comparing the present results with those obtained by the generic spectral method alone, we find that most of structures found by the generic spectral method are stable ones. This suggests that the generic spectral method is useful for the search of new structures. However, the discrepancies of the phase diagrams indicate that using the generic spectral method alone to determine phase diagrams is not efficient. The combination of the real-space method and the generic spectral method is a feasible strategy in the study of phase behaviors of complex block copolymers.

The star triblock copolymers have complex self-assembling behaviors in bulk. Our careful calculations and analysis are helpful to understand the self-assembling mechanism of polygonal structures as well as other interesting structures. However, there are still notable discrepancies between the theoretical predictions and experimental observations. It should motivate further investigations on the phase behaviors of the triblock copolymers in future. For example, in experiments of ISP triblock copolymers, the

three Flory–Huggins interactions are not equal and have the relation of $\chi_{IP} > \chi_{IS} \approx \chi_{SP}$. For this case of interactions, the phase diagram becomes more complicated than the present one because it has only one mirror symmetric axis. Therefore, its calculation increases from one-sixth to one-half of the whole triangular phase diagram. The present phase diagram is a useful guide for future calculations.

ACKNOWLEDGMENTS

This work was supported by the National Natural Science Foundation of China (Grant Nos. 20974026 and 20625413). W.L. gratefully acknowledges support from the Shanghai Pujiang Program (Program No. 08PJ1402000), the Shanghai Educational Development Foundation (Program No. 2008CG02), and the Scientific Research Foundation for the Returned Overseas Chinese Scholars, State Education Ministry.

[1] C. Park, J. Yoon, and E. L. Thomas, Polymer **44**, 6725 (2003).
[2] R. Ruiz, H. Kang, F. A. Detcheverry, E. Dobisz, D. S. Kercher, T. R. Albrecht, J. J. de Pablo, and P. F. Nealey, Science **321**, 936 (2008).
[3] I. Bita, J. K. W. Yang, Y. S. Jung, C. A. Ross, E. L. Thomas, and K. K. Berggren, Science **321**, 939 (2008).
[4] Y. Tada, S. Akasaka, H. Yoshida, H. Hasegawa, E. Dobisz, D. Kercher, and M. Takenaka, Macromolecules **41**, 9267 (2008).
[5] Y. Tada, S. Akasaka, M. Takenaka, H. Yoshida, R. Ruiz, E. Dobisz, and H. Hasegawa, Polymer **50**, 4250 (2009).
[6] W. H. Li, F. Qiu, Y. L. Yang, and A. C. Shi, Macromolecules **43**, 1644 (2010).
[7] M. W. Matsen and M. Schick, Phys. Rev. Lett. **72**, 2660 (1994).
[8] M. W. Matsen, J. Phys.: Condens. Matter **14**, R21 (2002).
[9] C. A. Tyler and D. C. Morse, Phys. Rev. Lett. **94**, 208302 (2005).
[10] C. A. Tyler, J. Qin, F. S. Bates, and D. C. Morse, Macromolecules **40**, 4654 (2007).
[11] T. Gemma, A. Hatano, and T. Dotera, Macromolecules **35**, 3225 (2002).
[12] Z. Guo, G. Zhang, F. Qiu, H. Zhang, Y. Yang, and A.-C. Shi, Phys. Rev. Lett. **101**, 028301 (2008).
[13] N. Hadjichristidis, H. Iatrou, S. K. Behal, J. J. Chludzinski, M. M. Disko, R. T. Carner, K. S. Liang, D. J. Lohse, and S. T. Milner, Macromolecules **26**, 5812 (1993).
[14] H. Hückstädt, V. Abetz, and R. Stadler, Macromol. Rapid Commun. **17**, 599 (1996).
[15] S. Okamoto, H. Hasegawa, T. Hashimoto, T. Fujimoto, H. Zhang, T. Kazama, and A. Takano, Polymer **38**, 5275 (1997).
[16] S. Sioula, Y. Tselikas, and N. Hadjichristidis, Macromolecules **30**, 1518 (1997).
[17] S. Sioula, N. Hadjichristidis, and E. L. Thomas, Macromolecules **31**, 5272 (1998); **31**, 8429 (1998).
[18] H. Hückstädt, A. Gopfert, and V. Abetz, Macromol. Chem. Phys. **201**, 296 (2000).
[19] K. Yamauchi, K. Takahashi, H. Hasegawa, H. Iatrou, N. Hadjichirstidis, T. Kaneko, Y. Nishikawa, H. Jinnai, T. Matsui, H. Nishioka, M. Shimizu, and H. Furukawa, Macromolecules **36**, 6962 (2003).
[20] A. Takano, S. Wada, S. Sato, T. Araki, K. Hirahara, T. Kazama, S. Kawahara, Y. Isono, A. Ohno, N. Tanaka, and Y. Matsushita, Macromolecules **37**, 9941 (2004).
[21] K. Yamauchi, S. Akasaka, H. Hasegawa, H. Iatrou, and N. Hadjichristidis, Macromolecules **38**, 8022 (2005).
[22] A. Takano, W. Kawashima, A. Noro, Y. Isono, N. Tanaka, T. Dotera, and Y. Matsushita, J. Polym. Sci., Part B: Polym. Phys. **43**, 2427 (2005).
[23] K. Hayashida, W. Kawashima, A. Takano, Y. Shinokara, Y. Amemiya, Y. Nozue, and Y. Matsushita, Macromolecules **39**, 4869 (2006).
[24] K. Hayashida, A. Takano, S. Arai, Y. Shinohara, Y. Amemiya, and Y. Matsushita, Macromolecules **39**, 9402 (2006).
[25] K. Hayashida, N. Saito, S. Arai, A. Takano, N. Tanaka, and Y. Matsushita, Macromolecules **40**, 3695 (2007).
[26] K. Hayashida, T. Dotera, A. Takano, and Y. Matsushita, Phys. Rev. Lett. **98**, 195502 (2007).
[27] H. Iatrou and N. Hadjichristidis, Macromolecules **25**, 4649 (1992).
[28] T. Fujimoto, H. Zhang, H. Kazanawa, X. Isono, H. Hasegawa, and T. Hashimoto, Polymer **33**, 2208 (1992).
[29] Y. Matsushita, Macromolecules **40**, 771 (2007).
[30] C. T. Huang, H. K. Fang, and C. H. Lin, Phys. Rev. E **77**, 031804 (2008).
[31] G. J. Zhang, F. Qiu, H. D. Zhang, Y. L. Yang, and A. C. Shi, Macromolecules **43**, 2981 (2010).
[32] A. C. Shi, in *Development in Block Copolymer Science and Technology*, edited by I. W. Hamley (Wiley, New York, 2004).
[33] G. H. Fredrickson, *The Equilibrium Theory of Inhomogeneous Polymers* (Oxford University Press, Oxford, 2006).
[34] F. Drolet and G. H. Fredrickson, Phys. Rev. Lett. **83**, 4317 (1999).
[35] G. Tzeremes, K. Ø. Rasmussen, T. Lookman, and A. Saxena, Phys. Rev. E **65**, 041806 (2002).
[36] K. Ø. Rasmussen and G. J. Kalosakas, J. Polym. Sci., Part B: Polym. Phys. **40**, 1777 (2002).
[37] E. W. Cochran, C. J. Garcia-Cervera, and G. H. Fredrickson, Macromolecules **39**, 2449 (2006).
[38] M. W. Matsen and F. S. Bates, J. Chem. Phys. **106**, 2436 (1997).
[39] Y. C. Xu, W. H. Li, F. Qiu, H. D. Zhang, Y. L. Yang, and A. C. Shi, J. Polym. Sci., Part B: Polym. Phys. **48**, 1101 (2010).
[40] P. Tang, F. Qiu, H. Zhang, and Y. Yang, J. Phys. Chem. B **108**, 8434 (2004).